PAPER • OPEN ACCESS

A compartmentalized neuron-oligodendrocyte co-culture device for myelin research: design, fabrication and functionality testing

View the article online for updates and enhancements.

You may also like

A compartmentalized neuron-oligodendrocyte co-culture device for myelin research: design, fabrication and functionality testing

Mervi Ristola[1,6,7,8], **Lassi Sukki**[2,8], **Maria Manuela Azevedo**[3,4],
Ana Isabel Seixas[3,4], **João Bettencourt Relvas**[3,4,5],
Susanna Narkilahti[1,8] **and Pasi Kallio**[2,8]

[1] Neuro Group, Faculty of Medicine and Health Technology, Tampere University, Arvo Ylpön katu 34, 33520 Tampere, Finland
[2] Micro- and Nanosystems Research Group, Faculty of Medicine and Health Technology, Tampere University, Korkeakoulunkatu 10, 33720 Tampere, Finland
[3] i3S—Instituto de Investigação e Inovação em Saúde, Universidade do Porto, Rua Alfredo Allen, 208, 4200-135 Porto, Portugal
[4] IBMC—Instituto de Biologia Molecular e Celular, Rua Alfredo Allen, 208, 4200-135 Porto, Portugal
[5] The Discoveries Centre for Regeneration and Precision Medicine, Porto Campus, Rua Alfredo Allen, 208, 4200-135 Porto, Portugal

E-mail: mervi.ristola@tuni.fi

CrossMark

Abstract

Microfluidics devices for co-culturing neurons and oligodendrocytes represent an important *in vitro* research tool to decipher myelination mechanisms in health and disease and in the identification of novel treatments for myelin diseases. In reported devices using primary rodent cells, the spontaneous formation of myelin sheaths has been challenging and random orientation of neurites impede the analysis of myelination. Furthermore, fabrication methods for devices show limitations, highlighting the need for novel *in vitro* cell-based myelination models. In the present study, we describe a compartmentalized cell culture device targeted for neuron-oligodendrocyte co-culturing and myelination studies. In the device, neurites from primary rat dorsal root ganglion (DRG) neurons were capable of forming aligned dense networks in a specific compartment that was physically isolated from neuronal somas. Co-culture of rat DRG neurons and oligodendrocytes, a well-known model to study myelination *in vitro*, led to interactions between oligodendrocytes and neurites in the device, and the deposition of myelin segments in an aligned distribution was spontaneously formed. For the fabrication of the device, we present a new method that produces polydimethylsiloxane (PDMS)—based devices possessing an open compartment design. The proposed fabrication method takes advantage of an SU-8 photolithography process and 3D printing for mould fabrication. Both the microscale and macroscale features are replicated from the same mould,

[6] Faculty of Medicine and Health Technology, Tampere University, Arvo Ylpön katu 34, 33520 Tampere, Finland
[7] Author to whom any correspondence should be addressed.
[8] Equal contribution.

allowing devices to be produced with high precision and repeatability. The proposed device is applicable for long-term cell culturing, live-cell imaging, and by enhancing aligned myelin distribution, it is a promising tool for experimental setups that address diverse biological questions in the field of myelin research.

S Supplementary material for this article is available online

(Some figures may appear in colour only in the online journal)

1. Introduction

Microfluidics devices are important and practical research tools for a variety of biological applications, including in the field of neuroscience and myelin research. Myelination is an essential biological process whereby oligodendrocytes in the central nervous system (CNS) and Schwann cells in the peripheral nervous system (PNS) form myelin sheaths around the axons of neurons, ensuring the proper functioning of the vertebrate nervous system [1]. The mechanisms underlying myelination, as well as the mechanisms that underlie myelin diseases such as multiple sclerosis and peripheral neuropathies, are still not completely understood. This is not only because myelination is a highly regulated process but also because studying myelination *in vivo* is complex and time-consuming; therefore, there is a crucial need for suitable *in vitro* cell-based models [2–5].

Traditional *in vitro* neuron and myelinating cell co-culture systems are typically implemented on cell culture plates, dishes or glass coverslips where the quantitation of myelin formation and changes is difficult due to randomly distributed neurites and the presence of neuronal cell somas [6]. Furthermore, these culture conditions differ vastly from the *in vivo* environment, where cellular functions, including myelination, are tightly controlled in a spatiotemporal manner [7–10]. To overcome these issues, compartmentalized neuron culture started with Campenot chambers [11]. The development in the field of microfabrication and microfluidics enabled the creation of next-generation compartmentalized devices. Microfluidics technology allows the fabrication of multi-compartment cell culture devices where microenvironmental conditions can be controlled spatially and temporally to better mimic *in vivo* conditions. Furthermore, defined compartments in devices can be used to monitor cellular and subcellular events and to ease experimental analysis [7–9]. To study the interactions and signalling between neurites and myelinating cells, microfluidics devices have been established to compartmentalize neurites and myelinating cells in a defined compartment separated from neuronal somas by microtunnels [12, 13]. However, the earlier works using devices from these pioneering studies in the culture of primary rodent cells have not concentrated on the establishment of aligned neurite culture and the spontaneous formation of myelin segments has been challenging [12–16]. Alignment of neurites may play a remarkable role in the success of myelination *in vitro*, as it has been reported that oligodendrocyte differentiation is enhanced on aligned polycaprolactone (PCL) fibers compared to random PCL fibers [17]. *In vivo* studies with nanofibrous nerve conduits have further shown thicker myelin sheaths on aligned conduits than on random conduits [18]. Furthermore, quantitation of myelination is difficult if neurites are randomly oriented in the culture. Thus, improvements in microfluidic devices for myelin research aiming to aligned neurite growth are needed.

Microfluidics devices used in *in vitro* research can be divided into so-called enclosed and open compartment designs, both of which have been utilized in myelin studies [4, 12–16]. Neural cells are often very sensitive to chemical and mechanical changes in their environment and cell-specific growth requirements need to be considered in device design and fabrication. In devices with an enclosed compartment design, low-height cell compartments are enclosed within polydimethylsiloxane (PDMS) and access to open medium reservoirs is only at the ends of the cell compartments. This can cause uncontrollable or even impossible cell seeding, undesirable shear forces and inefficient nutrient supply and waste removal that in case of neuronal cells may negatively affect cell growth [19–21]. By adopting an open compartment design, the negative effects of enclosed compartment design can be avoided, and better culture conditions as well as improved cell viability and neurite growth is possible [4, 20, 22, 23].

Two different methods to fabricate microfluidics devices possessing an open compartment design for myelination studies have been used in the past. In the most commonly used method, only the microscale features are included in an SU-8 mould [4, 13, 15, 16]. Because the open macroscale features of the device are created by manual cutting, the drawbacks of this fabrication method include poor control over open features and poor repeatability between devices [24]. Another fabrication method developed by Park *et al* exploits a method called micro-macro hybrid soft-lithography master (MMHSM) [24]. In the MMHSM method, both the microscale and macroscale features of the devices are replicated using a mould called a PMMA (poly(methyl methacrylate)) master. However, this method has a fairly complex fabrication process involving the fabrication of a replica device by milling macroscale features onto a PMMA piece, electroplating microscale features from copper onto a glass wafer and hot embossing these features onto the milled PMMA piece. This replica device is then used to mould the actual mould from PDMS. The PDMS mould is plasma bonded to a glass wafer and treated with (tridecafluoro-1,1,2,2-tetrahydrooctyl) trichloro-silane before it

can be used to mould PDMS replicas. To our knowledge, this method has not been adopted by other groups indicating its complexity. Thus, microfluidics devices with open compartments require alternative mould fabrication methods which share the simplicity of the traditional sole SU-8 based moulds and the repeatability of the MMHSM method.

In this study, we propose a compartmentalized co-culture device targeted for neuron-oligodendrocyte *in vitro* studies and a new SU-8 and 3D printing-based fabrication method that produces repeatably PDMS-based microfluidics devices with an open compartment design. We report the successful co-culture of primary rat dorsal root ganglion (DRG) neurons and oligodendrocytes in this microfluidics device, which can also be used for time-lapse imaging. We demonstrate successful interactions and contacts between oligodendrocytes and neurites, with the deposition of aligned myelin segments in the device.

2. Materials and methods

2.1. Design and fabrication of the microfluidics device

The co-culture microfluidics device (figure 1) contains three sequential compartments: two neuronal soma compartments (length = 3 mm, width = 4 mm) at the ends, which are interconnected by microtunnels to a compartment for neurite-oligodendrocyte interactions and myelination analysis in the middle (length = 3 mm or 5 mm, width = 4 mm). Primary rat neurons have previously cultured in the microfluidics devices with 200–500 μm microtunnel length for the separation of neurites from their cell somas [13, 15, 16, 25–27]. As shorter and a higher number of microtunnels in the microfluidics devices have shown to improve functional formation of neurite networks [13, 28], the microtunnel length was set to 250 μm and the number to 40 in our device. Two different microtunnel cross-sectional areas, tunnels 1.5 μm high and 5 μm wide and tunnels 3.5 μm high and 10 μm wide, were designed. All the dimensions of four different device designs evaluated in this study are summarized in table 1.

The mould for the fabrication of the device is comprised of (i) an SU-8 part that defines the microscale features, i.e. the microtunnels and the cell compartment areas, and (ii) three 3D-printed steel inserts that provide the open macroscale features for the device (figure 2). To accurately align and attach the SU-8 part and the inserts together, a pair of holes and a pair of pins were designed for the SU-8 part and the bottom of each 3D insert, respectively (figure 2). The SU-8 part was fabricated using multilayer SU-8 rapid prototyping methods, which have been described in detailed earlier [29]. Three chrome-on-glass masks, one containing the 5 μm wide microtunnels, one the 10 μm wide microtunnels and one with the three cell compartment areas, were designed using SolidWorks (SolidWorks Corp., Waltham, MA, USA). The masks were fabricated from mask blanks (Clean Surface Technology Co., Tokyo, Japan) using a direct writing device (μpg501, Heidelberg Instruments Mikrotechnik GmbH, Heidelberg, Germany). SU-8 5 and SU-8 3050 photoresists (micro resist technology GmbH, Berlin, Germany) were subsequently spin-coated on a silicon wafer (University Wafer, Boston, MA, USA) to produce two
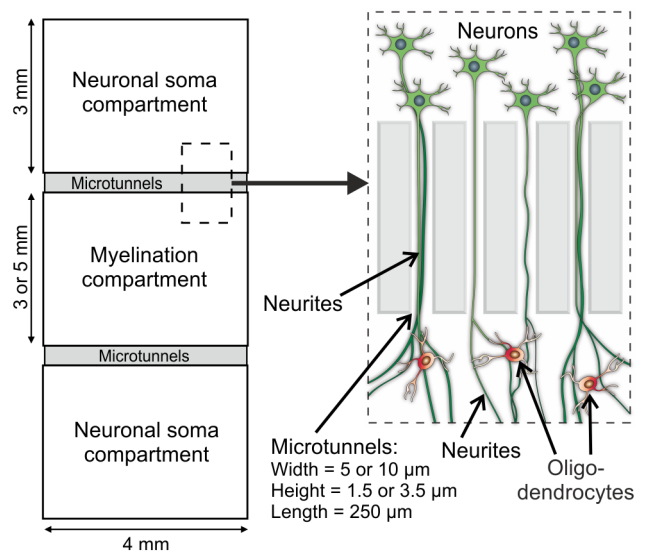

Figure 1. Schematic illustration of the compartmentalized cell culture device for neuron-oligodendrocyte co-culturing. The device consists of two neuronal soma compartments and a myelination compartment. The outer diameters for compartments are shown in the figure. The neuronal soma compartments are interconnected to the myelination compartment by 40 microtunnels with the dimensions shown in the figure. Enlargement of the device cartoon illustrates the purpose of the microtunnels to isolate neurites from their somas and guide them to the myelination compartment. In the myelination compartment, the neurite network is formed and oligodendrocytes can interact with and ensheath neurites in the absence of neuronal somas.

combined layers of different heights. Once the layer for the 1.5 μm-high or 3.5 μm-high microtunnels was developed, the second layer for the 200 μm-high cell compartment areas and alignment holes was fabricated on top of it. Before spin coating, the silicon wafers were treated with oxygen plasma at 30 W for two minutes in a reactive ion etcher (Vision 320 Mk II RIE, Advanced Vacuum, Malmö, Sweden). The 3D inserts with 3 mm height were designed with SolidWorks and printed from stainless steel 316L using selective laser melting (SLM) [30] with 25 μm layer height using 40 μm diameter laser beam (Materflow Oy, Lahti, Finland). The alignment pins of the inserts were designed for a height of 150 μm, and the outer dimensions of the inserts were designed to be 100 μm smaller than the corresponding cell compartment areas to take the manufacturing tolerance of 3D printing into account. To improve the PDMS demoulding, the insert sidewalls were designed at a 70° angle as previously reported [24], and the surfaces of the inserts that come into contact with PDMS were polished using fine grit sandpaper, up to P2000. A viscous steel epoxy was used to attach the inserts and the SU-8 parts by depositing the epoxy to a cavity (figure 2). The high viscosity of the epoxy prevented it from leaking out of the cavity as the insert was pressed for gluing onto the SU-8 mould.

The final PDMS device was fabricated from two PDMS parts: (1) a cell chamber part containing the microtunnels and cell compartments and (2) a medium reservoir chamber containing additional cell culture medium which allows for a longer interval between medium changes (figure 2). The cell

Table 1. Dimensions of devices and number of devices used in the experiments.

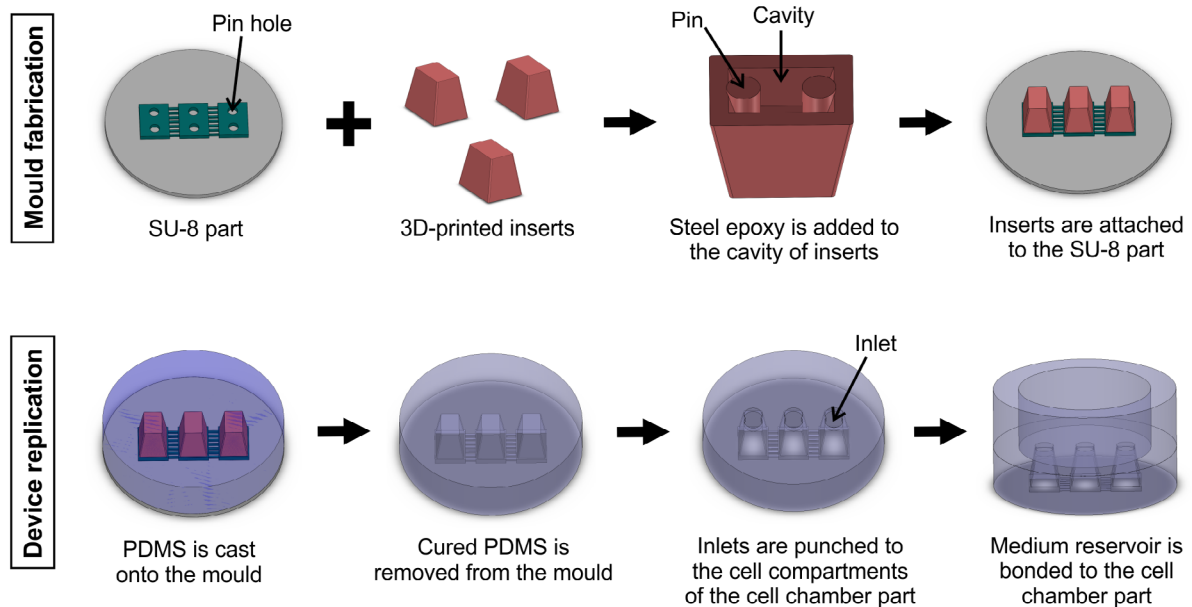| Device name	Microtunnels			Myelination compartment		Number of devices	
	Height (μm)	Width (μm)	Length (μm)	Length (mm)	Width (mm)	Cell culture	Immunostaining
3.5/10 μm_3 mm	3.5	10	250	3	4	7	6
3.5/10 μm_5 mm	3.5	10	250	5	4	8	6
1.5/5 μm_3 mm	1.5	5	250	3	4	7	6
1.5/5 μm_5 mm	1.5	5	250	5	4	8	4

Figure 2. Fabrication steps for the microfluidics cell culture device for neuron-oligodendrocyte co-culturing. The mould is fabricated from an SU-8 part, which defines the microscale microtunnels and cell compartment areas, and three 3D-printed inserts, which provide the open macroscale features. For the accurate alignment, the inserts contain two pins on the bottom that match into pin holes in the SU-8 part. The SU-8 part and 3D inserts are attached together by placing steel epoxy into the cavity on the bottom of the inserts and aligning them to the SU-8 part. The final PDMS device is fabricated from two PDMS parts: a cell chamber part and a medium reservoir. The cell chamber part is replicated from the fabricated mould. To connect the neuronal soma and myelination compartments to the medium reservoir, inlets are punched for each compartment. A medium reservoir chamber is produced from the PDMS sheet by punching and bonded to the cell chamber part using oxygen plasma.

chamber was replicated from the fabricated mould by carefully pouring degassed PDMS into the mould. After curing in the oven, the PDMS was slowly and carefully removed from the mould. Each cell chamber was separated from a PDMS replica containing six cell chambers using a ⌀24 mm biopsy punch. To connect the cell compartments in the cell chamber to the medium reservoir, inlets (figure 2) were punched for each compartment using either a ⌀2 mm or a ⌀3 mm biopsy punch, depending on the compartment size. The medium reservoir part of the device was fabricated from a 8 mm thick PDMS sheet using biopsy punches to provide a wall width of approximately 4.5 mm. The maximum holding capacity of the medium reservoir for liquid is approximately 1.4 ml. The medium reservoir chamber was bonded onto the cell chamber part using oxygen plasma (Pico, Diener electronic GmbH + Co. KG, Ebhausen, Germany) for 20 s at 30 W and 0.3 mbar pressure.

The microtunnels and cell compartments in the final PDMS device were coated with polyvinylpyrrolidone (PVP) to make them permanently hydrophilic and facilitate the supply of Matrigel as well as the cell culture medium in

the microscale features when preparing the devices for cell culture. A modified PVP coating protocol was used for the treatment [31]. Briefly, the device was reversibly bonded to a glass wafer with the features against the glass and was then treated with oxygen plasma for five minutes at 30 W and 0.3 mbar pressure. After the plasma treatment, the microtunnels and cell compartments were filled with a PVP solution (22.2% (w/v) solution containing polyvidone 25 powder (Merck, Kenilworth, NJ, USA) mixed with deionized (DI) water (Direct-Q3, Merck)) for ten minutes, washed with DI-water and dried using pressurised air.

2.2. Characterization of the mould and microfluidics device

Before attaching the 3D-printed inserts to the SU-8 parts, the dimensions of the SU-8 parts were characterized using a contact profilometer (Dektak XT, Bruker, Billerica, MA, USA) by measuring the heights of the microtunnels and the cell compartment areas. A scanning electron microscope (SEM, Zeiss ULTRA-55, Carl Zeiss AG, Oberkochen, Germany) was used

to characterize the PDMS devices. The PDMS devices used in SEM imaging were taken from the last fabrication batch that was the fifth batch. Thus, the moulds had been used multiple times prior making devices to imaging allowing observation of possible wearing of the mould. The devices were bonded to microscope slides using oxygen plasma bonding and then coated with 10 nm of gold using metal vapour deposition. The microtunnels and the walls between the cell compartments were selected as structures to be imaged. The analysis included 33 images of the 10 μm wide tunnels from one device to study how accurately our method replicates microscale features. The analysis was done using GNU image manipulation program (GIMP), where the widths of the features were measured using the measure tool. This tool provides widths in pixels, which was multiplied by pixel size information provided by the SEM. Both width mean and standard deviation were calculated in MATLAB (The MathWorks, Inc, MA, USA).

2.3. Preparation of microfluidics devices for cell culture

Glass coverslips ($\varnothing$24 mm) were coated with 25 μg/ml poly-D-lysine (PDL) (#P7405, Sigma-Aldrich, St. Louis, MO, USA) diluted in boric acid buffer for two hours at RT. Uncoated PDL was removed by washing with sterile H_2O and the coverslips were allowed to air-dry. The PVP-coated PDMS devices were sterilized by immersing them into 70% ethanol and air-drying thereafter to remove the residual ethanol. The devices were then attached to PDL-coated coverslips by reversible bonding. Reversible bonding was preferred over permanent bonding because of its simplicity and because oxygen plasma treatment needed in permanent bonding may have negative effect on the PDL coating of the coverslip. Neuronal soma compartments, myelination compartments and microtunnels of bonded devices were immediately filled with Matrigel (#354234, Enzifarma, Lisbon, Portugal) diluted at 1:20 that was the dilution specifically optimized for the devices. Dilution was made in Dulbecco's Modified Eagle's medium (DMEM) including high glucose, GlutaMAX and sodium pyruvate (#31966047, Invitrogen, Thermo Fisher Scientific, Rockfore, IL, USA) and coatings were performed for 3 h at 37 °C. The number of four different device designs included in the study is shown in table 1. The devices were kept in 6-well cell culture plates. Control cultures were performed on glass coverslips ($\varnothing$14 mm) treated with the same coatings as for the devices with the exception that the Matrigel dilution was 1:10 according to the standard protocol for rat DRG neurons and oligodendrocyte co-culture [32].

2.4. Animals and primary cell preparation

Wistar rats were used for the preparation of primary cultures of dorsal root ganglia (DRG) neurons and mixed glial cells (MGCs). DRGs were isolated from spinal cords of E15 rat embryos as previously described [32, 33]. Oligodendrocyte precursor cells (OPCs) were isolated from MGCs from postnatal day 0-2 (P0-P2) rat brains as previously described [32, 34, 35]. All animal experiments were performed with

approval from and in accordance with the IBMC/i3S Animal Ethics Committee, the Portuguese Veterinary Office and the European Union animal welfare laws and guidelines.

2.5. Rat DRG neuron and oligodendrocyte myelinating co-cultures

Purified DRG neurons can be myelinated by oligodendrocytes and their co-culture represents the most used myelination model *in vitro* [36–39]. Myelinating co-cultures were established as previously published with minor modifications [32, 33]. Before plating the DRG neurons into the PDMS device, Matrigel was pipetted out of the compartments, and the compartments were equilibrated with DMEM (including high glucose, GlutaMAX and sodium pyruvate; #31966047, Invitrogen, Thermo Fisher Scientific) supplemented with 10% fetal bovine serum (FBS) (Gibco, Thermo Fisher Scientific) and 1% penicillin/streptomycin (Thermo Fisher Scientific), named complete DMEM (C-DMEM). Dissociated DRG neurons were suspended in C-DMEM with nerve growth factor (NGF, 100 ng/ml; #13290010, Thermo Fisher Scientific) and seeded into the both neuronal soma compartments at a density of 1250–2100 cells mm^{-2} in a volume of 15 μl that fits into the compartment. For the control co-cultures, 90 000 neurons were plated on $\varnothing$14 mm coverslips. Neurons were allowed to attach overnight in a humidified incubator at 37 °C and 5% CO_2. The next day, 500 μl of C-DMEM supplemented with NGF was added to the cultures. Cultures were treated at 1, 2 and 3 days *in vitro* (DIV) for 8 h with 5-fluoro-2'-deoxyuridine (FUrd, 20 μM; #F0503, Sigma-Aldrich) that is an antimitotic agent and removes the proliferating non-neuronal cells but maintains neurons in the culture. After 3 DIV, FBS in C-DMEM was replaced with 1% B27 (#0080085SA, Invitrogen, Thermo Fisher Scientific) and the cultures were grown for 21 DIV with total media (500 μl) changes every 2–3 d. After 21 DIV, OPCs were seeded on top of the isolated neurite network in the myelination compartment of the device at a density of 80-125 cells mm^{-2} and on top of the neurons in the control culture (10 000 OPCs/coverslip). The co-cultures were maintained in myelinating medium (SATO medium (DMEM/F12 (Sigma-Aldrich) supplemented with insulin (5 mg ml^{-1}; Sigma-Aldrich), human apo-transferrin (100 μg ml^{-1}; Sigma-Aldrich), BSA (100 μg ml^{-1}; NZYTech, Lisbon, Portugal), progesterone (60 ng ml^{-1}; Sigma-Aldrich), putrescine (16 μg ml^{-1}; Sigma-Aldrich), sodium selenite (40 ng ml^{-1}; Sigma-Aldrich), thyroxine (40 ng ml^{-1}; Sigma-Aldrich), triiodo-L-thyronine (30 ng ml^{-1}; Sigma-Aldrich)) completed with 1% B27, NGF (100 ng ml^{-1}), N-acetyl-L-cysteine (5 ng ml^{-1}; Sigma-Aldrich), and D-biotin (10 ng ml^{-1}; Sigma-Aldrich)) for additional 18 DIV with total media (500 μl) changes every 2–3 d.

2.6. Time-lapse microscopy

Live-cell imaging of the co-cultures in the PDMS devices was performed with phase-contrast microscopy. The devices were imaged on a 6-well plastic bottom plate with 150 s intervals

for 1.5 d after the addition of OPCs. All images were recorded under a controlled environment (37 °C and 5% CO_2) with a Zeiss Axiovert 200M microscope (Carl Zeiss AG) equipped with an A-Plan 20×/0.30 Ph1 objective and a Roper Coosnap HQ camera. For each device, a region of interest (ROI) was defined using the 'create ROI grid' option in Micromanager 1.4 [40] image acquisition software. For some of the still images, false colouring was used for the visualization of oligodendrocytes in Adobe Photoshop (version 20161012.r.53).

2.7. Immunofluorescence

For assessing the identity of the cells and myelin formation in the co-cultures, immunocytochemical staining was performed following a previously published protocol with minor modifications [32, 41]. Briefly, cells were fixed in microtubule-protecting fixative buffer (MP-PFA; 4% PFA, 65 nM PIPES, 25 mM HEPES, 10 mM EGTA and 3 mM $MgCl_2$ in PBS) for 40 min at room temperature (RT), followed by permeabilization and blocking (in 1% HEPES buffer, 2.5% Triton X-100, 1% normal goat serum (NGS) and 1% normal horse serum in PBS) for 30 min at RT. Primary antibodies (rat anti-myelin basic protein (MBP), dil. 1:100 (#MCA409S, Bio-Rad Laboratories, Hercules, CA, USA) and mouse anti-βIII-tubulin, dil. 1:1000 (#302302, Synaptic Systems, Goettingen, Germany)) and secondary antibodies (goat anti-rat Alexa568, dil. 1:1000 and goat anti-rabbit Alexa488, dil. 1:1000 (#A21247 and #A11034, respectively; both from Molecular Probes, Thermo Fischer Scientific)) were diluted in blocking solution and sequentially incubated for 1 h at RT. After washing, the cells were incubated with DAPI dye (4′,6′-diamidino-2-phenylindole, dilactate; dil. 1:40 000, #D3571, Molecular Probes, Thermo Fisher Scientific) for nuclear staining for 15 min at RT. After washing, the coverslips were mounted with Fluoroshield mounting medium (Sigma-Aldrich). Imaging was performed on a Leica DMI6000 epifluorescence microscope (Leica, Wetzlar, Germany) using a 20×/0.40 CORR Ph1 or a 40×/0.60 objective equipped with an Orca Flash 4.0 v2.0 camera (Hamamatsu, Hamamatsu City, Japan). The number of devices in immunocytochemical analysis is shown in table 1. Image processing using a Gaussian blur filter and a nonlinear gamma change in Fiji software [42] was performed to enhance the image contrast for visualization purposes only.

2.8. Neurite orientation analysis

Fluorescence images immunostained with βIII-tubulin antibody were analysed for neurite orientation. The plugins OrientationJ Distribution [43] and OrientationJ Measure [44] in the ImageJ software (version 1.52e) were used to study the distribution and direction of neurite orientation, respectively, in the myelination compartment of the devices. Neurites aligned parallel to the direction of microtunnels were defined to be at 0° orientation and the other directions obtained angles in the range between −90° and +90°. Results are shown at the range from 0° to 90°, as absolute values of orientation angles were considered. Weighted histograms of neurite orientation

distribution were built based on the normalized frequencies of pixel orientations at 15° intervals. Spectral analysis software CytoSpectre [45] was used for the quantitative analysis of neurite distribution in the devices compared to the control culture freely growing on a glass coverslip as previously described [46, 47]. The software calculates the orientation distribution as a circular variance value, where 0 indicates completely unidirectional orientation and 1 random distribution of orientation. Maximum wavelength was set to 20 μm to analyse neurites but to exclude somas from the analysis. All data for statistical analyses was found to be non-normal and therefore the nonparametric Mann–Whitney *U*-test was used. Statistical analyses were performed using SPSS Statistics (v.25; IBM Corp., Armonk, NY, USA) and a *p*-value less than 0.05 was considered statistically significant.

3. Results and discussion

3.1. Fabrication and characterization of the mould and the microfluidics device

Microfluidics devices were fabricated using the method proposed here (figure 2). For the cell experiments, 32 devices were fabricated with a success rate of approximately 90% of the devices remaining intact after demoulding. Most failures were caused due to the damage of the wall between the compartments in the demoulding process. The contact profilometer characterization of the SU-8 parts of the mould proved that they were successfully fabricated and the features in the SU-8 parts had the intended dimensions. The 3D-printed inserts were successfully attached to the SU-8 part with the help of the alignment pins and holes using two-component steel epoxy. The combination of the SU-8 part and the 3D-printed insert formed a mould for PDMS device replication (figure 3(a)). To analyse the quality of the PDMS devices and possible wearing of the mould, the PDMS devices were selected for SEM analysis from the fifth batch of the devices fabricated with the mould. As observed from the SEM images, the devices remained unbroken during the demoulding process, and the devices precisely replicated features from the mould, with accurate replication of the microtunnels (figure 3(b)). The measurements derived from SEM images of device with 10 μm microtunnel width indicated a mean tunnel width of 9.85 μm with a standard deviation of 0.09 μm. As the width was designed to be 10 μm, the measured width was only 1.5% smaller and thus within the range of PDMS shrinkage commonly considered to be 1%–3% due to heat [48]. The coefficient of variation was below 1% indicating excellent precision of the manufacturing process. Variations can be explained by some inaccuracy in image analysis due to the slightly blurry edges of the tunnels in the SEM images. The SEM images of the devices showed no indication of any wearing of the mould, implying that the mould can be reused several times. After this study, the moulds remained in active use, until degradation in device quality was noticed. This was caused by small PDMS fragments that were stuck between the inserts and the SU-8 parts in the mould. We estimate that the moulds fabricated with our method can be used
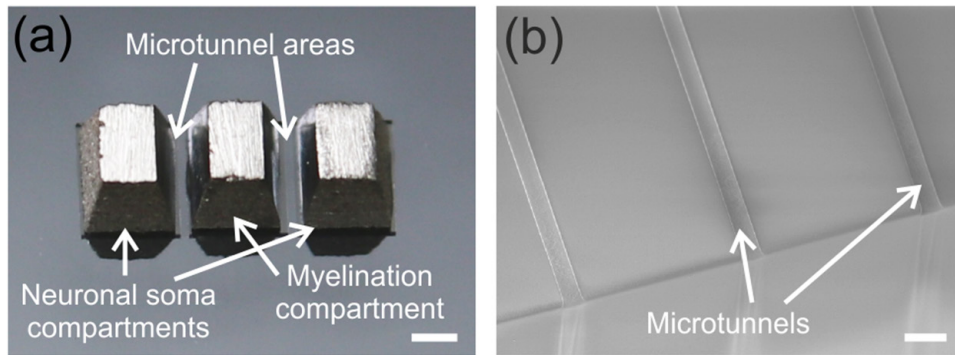
Figure 3. Characterization of the mould and the microfluidics PDMS device. (a) Fabricated mould imaged by Canon's system camera showing the 3D-printed inserts attached to the SU-8 part of the mould on the silicon wafer. Scale bar is 2 mm. (b) An SEM image showing the accurate replication of the microtunnels that are 3.5 μm in height and 10 μm in width. Scale bar is 20 μm.

approximately 15 times before degradation becomes significant. In the future work, the durability of the moulds can be improved by applying coating, such as (tridecafluoro-1,1,2,2-tetrahydrooctyl) trichloro-silane, which is occasionally used with moulds to improve demoulding [49].

In previous studies, two fabrication methods for microfluidics PDMS devices with open compartments have been presented. The method that uses an SU-8 mould for the microscale features and the manual cutting of the PDMS for the open features using either a biopsy punch or a scalpel is the most commonly used [4, 13, 15, 16]. However, developing more repeatable methods that use a single mould to produce all the features in the device is a matter of great importance. This kind of method has been presented only by Park *et al* [14, 24]. In their MMHSM method, a mould for the final PDMS device is first made from a PMMA master that is fabricated using a combination of milling for macroscale features and hot embossing for microscale features [24]. The MMHSM method allows the fabrication of both the microscale and macroscale features at the same time, thus being a controlled and repeatable method. However, the production of the final PDMS device requires two replication steps from the original mould that complicates the process and increases the dimension alterations caused by PDMS shrinkage. Other limitations of their MMHSM method include a requirement for special equipment and the complexity of the PMMA master fabrication. Thus, to the best of our knowledge, it has not been adopted by others. We proposed here an alternative fabrication method for microfluidics PDMS devices with open compartments. In our method, both the microscale and macroscale features are replicated using the same mould, thus sharing some similarities with the MMHSM method [24]. Our fabrication process, however, allows for combining multiple microscopic features of different heights with macroscopic features that is not possible with the MMHSM method. Furthermore, our method provides a simpler way to produce the mould by taking the advantages of a traditional SU-8 lithography process and 3D printing, and the final PDMS device requires only one replication step. Thus, by using the fabrication method proposed in this study, more complex microscopic features can be created and microfluidics devices can be produced faster and with a smaller number of process steps.

This is, to the best of our knowledge, the first study combining SU-8 lithography and 3D printing in the mould fabrication of a PDMS device. In earlier studies, the entire mould has been 3D printed. However, due to printing method limitations, the smallest dimensions have been in a range of hundreds of micrometres [50]. It has been suggested that the resolution limits of 3D printing could be mitigated by taking advantage of shrinkage in certain elastic resins. However, it has not been shown whether this kind of method is capable of producing both micrometre and millimetre scale features simultaneously in all three dimensions [51]. Thus, 3D printing as the only mould fabrication method is unable to produce sufficiently small microscale features in the devices containing also millimetre scale features. In our study, SLM was used as the 3D printing method due to the high quality and nonporous nature of SLM prints [30]. An SLM print was shown for the first time to be compatible with an SU-8 mould in the mould fabrication of PDMS devices. However, any fabrication method producing solid parts with sufficiently high accuracy, repeatability and surface quality is compatible with our method. Photolithography provides a large range for the width and the length of features, and it is possible to fabricate even sub-micrometre and millimetre sized features simultaneously [29, 52]. The downsides of photolithography are its limitations in the feature height (hundreds of micrometres) and the fabrication of devices with multiple different heights increases the duration and complexity of the fabrication process [52, 53]. Combining 3D printing with photolithography allows a significantly larger range of feature heights. Thus, the mould fabrication method presented in this study is highly applicable to meet the specific requirements of cell cultures in different research questions.

3.2. Neurite extension and orientation in the microfluidics device

This study aimed to build a cell culture device that promotes the formation of aligned-oriented neurite networks isolated from neuronal somas enabling easier analysis of myelination *in vitro*. A three-compartment design where the neurites extend into the middle compartment between two neuronal populations was created (figure 1). Rat DRG neurons were

chosen for cell culture as they have been broadly used and are considered as an invaluable research model for studying axonal biology as well as myelination [54–56]. DRG neurons from both embryonic and postnatal rats have been successfully cultured in microfluidics PDMS devices where the separation of neurites from their cell somas has been achieved using 450–500 μm-long microtunnels [15, 16, 25–27]. Reports on other rodent neuron types have shown that even a 200 μm microtunnel length is sufficient to isolate neurites from their somas [13]. Furthermore, shorter microtunnels and a higher number of microtunnels have the advantage of faster functional formation of extensive neurite networks compared to longer microtunnels and a lower number of microtunnels [13, 28]. In our device, the microtunnel length was set to 250 μm and the number to 40 so that these features would not be the limiting factors and would maximize the formation of a dense neurite network. With respect to the segregation of neurites from their cell somas, other microtunnel dimensions, the width and height, were taken into consideration in this study. Thus, two different microtunnel sizes, height = 3.5 μm × width = 10 μm and height = 1.5 μm × width = 5 μm, were tested for the culture of rat DRG neurons. Furthermore, devices with two different myelination compartment lengths, 3 mm and 5 mm, were included in the experiment to assess its effect on the neurite network formation.

In this study, dissociated DRG neurons seeded into the neuronal soma compartments started to extend their neurites into the microtunnels as early as 48 h after cell plating in all devices regardless of the microtunnel size or myelination compartment length. As the culture continued, neurites traversed the microtunnels and came out into the myelination compartment. The evaluation with phase-contrast microscopy and DAPI staining revealed hardly any DRG somas in the myelination compartment and the isolation of neurites from cell somas was observed with both tunnel sizes and both myelination compartment lengths (figures 4(a)–(d)). However, the behaviour of neurites in the myelination compartment differed depending on the size of the microtunnels. In the devices with larger microtunnels (height = 3.5 μm × width = 10 μm), neurites looked healthy and continued their extension into the myelination compartment towards the opposite neuronal soma compartment (figures 4(a) and (b)). Neurites formed in the myelination compartment of 3 mm length aligned and dense network (figure 4(a)), whereas in the 5 mm long myelination compartment the aligned network appeared sparser (figure 4(b)). Orientation analysis using OrientationJ Distribution showed that the majority of neurites in the myelination compartment of 3 mm length displayed a preferred direction in terms of orientation angle close to the 0° that was the defined direction of microtunnels (64% in the range from 0° to 30°; figure 4(e)). Neurites in the 5 mm long myelination compartment also exhibited a preferred direction parallel to the microtunnels but with a smaller percentage than in the 3 mm long myelination compartment (52% in the range from 0° to 30°; figure 4(f)). In the devices with smaller microtunnels (height = 1.5 μm × width = 5 μm), neurites were unable to extend along the myelination compartment of both 3 mm and 5 mm length. Neurite extension was nonlinear related to

the direction of the microtunnels and the appearance of neurites was curvy in front of the microtunnels, with only some neurites capable of reaching the opposite microtunnels in the myelination compartment (figures 4(c) and (d)). OrientationJ Distribution analysis showed that neither in the myelination compartment of 3 mm nor 5 mm length neurites had a preferred direction parallel to the microtunnels (figures 4(g) and (h)).

To further study the differences in neurite orientation in the myelination compartment of devices with different dimensions, orientation angles using OrientationJ Measure analysis were compared. The medians of neurite orientation angles in the devices with larger microtunnels (height = 3.5 μm × width = 10 μm) were 17° and 14° for 3 mm and 5 mm long myelination compartment, respectively (figure 4(i)). These values were significantly smaller ($p < 0.001$) than the corresponding medians in the devices with smaller microtunnels (height = 1.5 μm × width = 5 μm) that were 58° and 40° (figure 4(i)). As 0° is the defined direction of microtunnels, neurite orientation in the devices with larger microtunnels was confirmed to be aligned along the tunnel direction. Furthermore, a high variation in orientation angles in the devices with smaller microtunnels indicated random neurite orientation (figure 4(i)).

To further quantify the neurite alignment in the devices and in the control culture (figure 4(k)), circular variance was analysed using CytoSpectre software. The analysis showed median circular variances of 0.43 and 0.44 for the devices with larger microtunnels in 3 mm and 5 mm long myelination compartment, respectively (figure 4(j)). The values were significantly smaller ($p < 0.001$) than in the devices with smaller microtunnels (0.81 and 0.88 for 3 mm and 5 mm long myelination compartment, respectively) or in the control culture (0.67; figure 4(j)). As perfect alignment has a circular variance value of 0 and random alignment a value of 1, the analysis verified the presence of aligned neurite network in the myelination compartment with larger microtunnels.

In this study, an extensive comparison of device parameters and their quantitative analysis showed that in the devices with larger microtunnels (height = 3.5 μm × width = 10 μm), neurite extension of rat DRG neurons was aligned and parallel with the direction of microtunnels in the myelination compartment (figure 4). This tunnel size enabled robust neurite outgrowth at the same time with the isolation of neurites from their somas. The formed aligned neurite network appeared denser in the myelination compartment of 3 mm length than in the compartment of 5 mm length. We showed that neurite extension was limited and neurites had no preferred direction along the microtunnels in the device with smaller microtunnel size (height = 1.5 μm × width = 5 μm). Peyrin *et al* had similar findings with mouse cortical cells for narrow and long microtunnels (height = 3 μm, width < 3 μm, length = 500 μm) as neurite extension and integrity were reduced [57]. They further showed that the number of neurites passing through the microtunnels highly correlates to at least the width of the microtunnel; decreasing the tunnel width reduces the number of neurites exiting the tunnels [57]. Thus, the limited neurite extension ability in our study
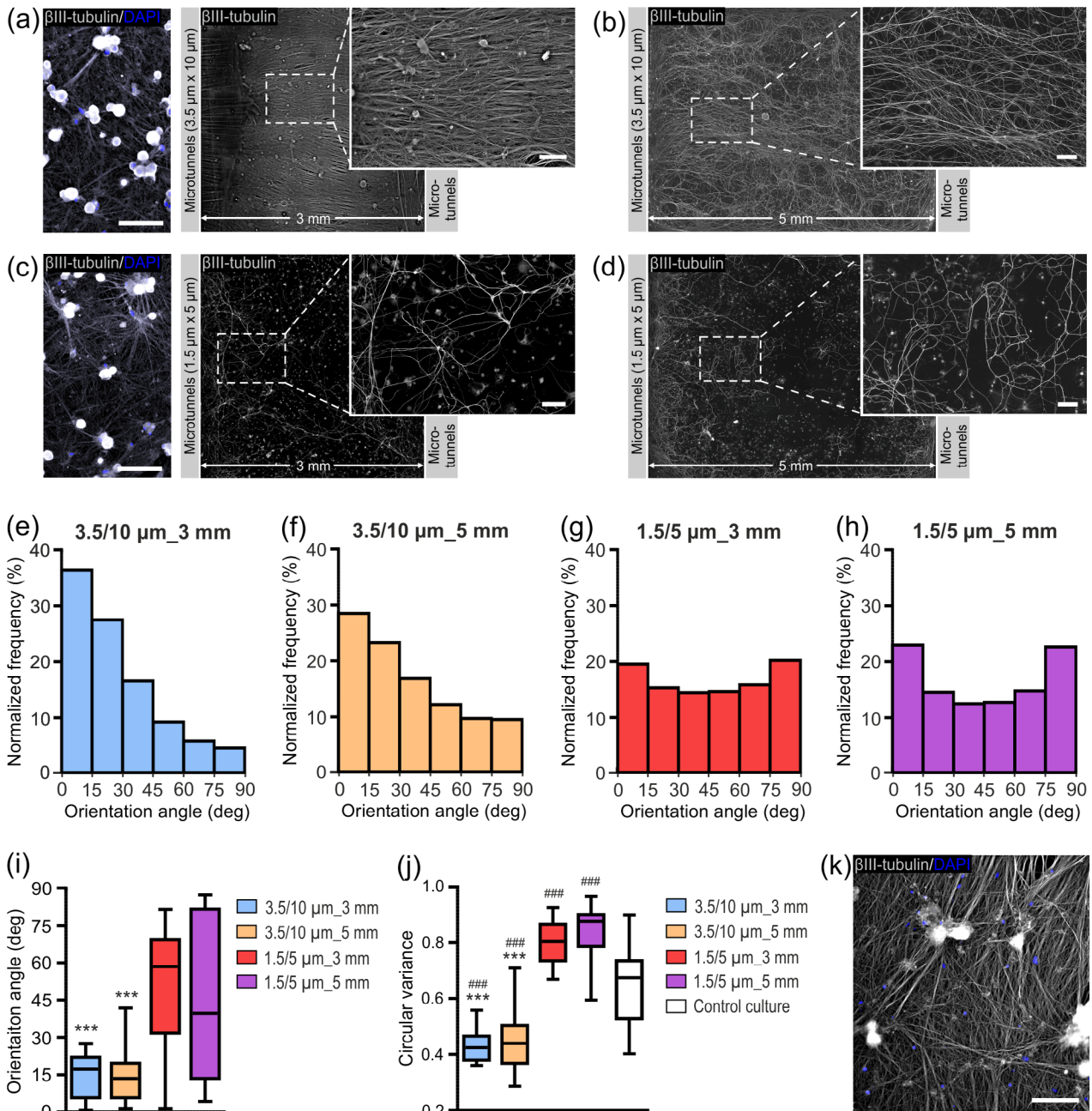
Figure 4. Neurite extension and orientation in the microfluidics device. (a) and (b) Neurites of rat DRG neurons formed aligned network in the myelination compartment of the device with larger microtunnels (height = 3.5 μm × width = 10 μm) whereas (c) and (d) neurite extension was impeded in the myelination compartment with smaller microtunnels (height = 1.5 μm × width = 5 μm) as shown by immunocytochemical staining with βIII-tubulin antibody. With both tunnel sizes, microtunnels isolated cell somas from neurites in all four device designs (representative images shown only for one soma compartment in (a) and (c)). Scale bars are 100 μm. (e)–(h) Weighted histograms of neurite orientation angle distributions in the devices with larger (height = 3.5 μm × width = 10 μm) and smaller (height = 1.5 μm × width = 5 μm) microtunnels and 3 mm or 5 mm long myelination compartment obtained with OrientationJ Distribution analysis. Normalized frequencies of pixel orientations are shown at 15° intervals and the direction of microtunnels is defined as 0° (horizontal axis of the images in (a)–(d)). (i) The quantitative analysis of neurite orientation angles relative to the direction of microtunnels (0°; horizontal axis of the images in (a)–(d)) with OrientationJ Measure function confirmed significantly aligned neurite network parallel to the direction of microtunnels in the devices with larger microtunnels compared to the devices with smaller microtunnels. (j) The quantitative analysis of neurite alignment confirmed significantly smaller circular variances of the neurite network in the devices with larger microtunnels than in the control culture of freely growing cells on a coverslip or in the devices with smaller microtunnels. (k) Immunostained image of control culture with βIII-tubulin antibody. Scale bar is 100 μm. In (e)–(j), 20 ROIs (20 single images with 20 × objective, each 512 μm × 512 μm) from 1–2 independent devices were examined. In (i) and (j), statistical analyses were calculated using the Mann–Whitney U-test and *symbols indicate significant differences compared to both the 1.5/5 μm_3 mm and 1.5/5 μm_5 mm devices (***$p \leqslant 0.001$) and #symbols compared to the control coverslip (###$p \leqslant 0.001$).

could be affected by the fewer number of neurites traversing together or the smaller microtunnel size may pose as a spatial obstacle that limits neurite extension.

We showed that neurites had no preferred direction in the devices with smaller microtunnel size (height $= 1.5$ μm $\times$ width $= 5$ μm). Interestingly, the analysis of circular variance between these devices and the control culture indicated that neurites in the control culture were more aligned (figure 4(j)). This can be due to the limited neurite extension in the devices. In the control culture, neurite density appeared to be very high (figure 4(k)). Even though neurites can extend into any direction, it can be that they tend to keep certain directions in this dense network. In contrary, the number of neurites seemed to be very low due to the poor neurite extension in the middle compartments of the devices with smaller microtunnels (figures 4(c) and (d)). Neurites with limited extension ability and low density most probably start to interact with other neurites that come from the parallel microtunnels. This leads to the curvy appearance of neurites in front of the microtunnels and more variable alignment than in the control culture.

Altogether, the data obtained in this study showed that the three-compartment device design with a specific microtunnel size and number, and the compartment size leads to a significant directional growth of neurites. Compared to the random growth of neurites in previous microfluidics PDMS devices designed for the co-culture of neurons and oligodendrocytes [4, 12–16], an aligned neurite network is a remarkable improvement.

3.3. Myelin formation in the microfluidics device

To assess the suitability of the established microfluidics PDMS device for the co-culture of neurons and oligodendrocytes and myelination studies, primary rat OPCs were co-cultured with DRG neurite network. The co-culture system of purified DRGs and oligodendrocytes is well-known and the most used model for studying myelination *in vitro* [36–38]. On DIV 21, OPCs were added on top of the isolated DRG neurite network formed in the myelination compartment during the initial culture period. OPC seeding did not disturb the existing neurite network and OPCs distributed uniformly on top of the aligned neurites. Following their addition, OPC processes started to contact and survey the neurites (figure 5(a) and supplementary movie 1 (stacks.iop.org/JMM/29/065009/mmedia)). Oligodendrocyte myelination capacity was assessed by the presence of MBP segments deposited on the neurites. After 18 days in co-culture, the oligodendrocytes were able to form MBP segments along the neurites as demonstrated by the overlap of MBP- and βIII-tubulin-positive staining (figure 5(b)). The myelin segment distribution followed the neurite network distribution in an aligned configuration (figure 5(b)). The differences in the appearance of myelination are evident when compared to the control co-culture where myelin sheaths were randomly distributed (figure 5(c)).

Microfluidics PDMS devices have been previously demonstrated for the co-culture of primary rodent neurons and oligodendrocytes [12–16]. However, the aligned distribution

of myelinated axons has not been in the focus of these studies and the spontaneous formation of myelin has been challenging in the devices. In the device with rat cortical neurons and oligodendrocytes, only the localization of oligodendrocytes along neurites was detected but no MBP-positive segments around neurites [12]. Similar results were also shown in the studies using a co-culture of rat CNS neurons and oligodendrocytes [13, 14]. To the best of our knowledge, the study using mouse embryonic stem cells as the cell source is the only one where spontaneous compact myelin formation has been shown in a microfluidics device [4]. In the studies with rat DRG neurons and oligodendrocytes, compact myelin sheaths have been shown only with the use of electrical stimulation [15, 16]. The previous studies have reported neither neurites nor myelin segments distributed in an aligned manner in the device. Our established device was thus proven to be advantageous over the reported devices, as we detected the spontaneously formed MBP segments along aligned neurites.

The design of the microfluidics device and prevailing microenvironment can make a difference for cells regarding their behaviour and myelination capability. Similar to our established device, the previously presented devices [13–16] represent open compartment designs, however, which are produced with different fabrication methods. All these devices have a so-called two-compartment design with respect to co-culture having thus geometric differences compared to our device. Microfluidics devices with multi-compartment designs have been published earlier [58–60] but they have not been used in myelination studies and their layout differ from our device. In our device, the number of microtunnels was chosen to be high enough because the higher number of microtunnels, hence the higher number of neurites, have been shown to have the advantage of faster functional formation of extensive neurite networks [28]. Importantly, functional activity of neurons has been reported to influence myelination process *in vitro* and *in vivo* [15, 16, 61]. The position of the three compartments in our device was sequential, that may have effect on promoting the establishment of an aligned neurite network in the myelination compartment. The use of aligned polycaprolactone (PCL) fibers and nanofibrous nerve conduits have shown enhanced oligodendrocyte differentiation [17] and thicker myelin sheaths [18], respectively, compared to their randomly oriented counterparts. Thus, neurite alignment and dense neurite network is suggested to maximize the potential for myelination seen in our device. As shown, our device supported interactions and contacts between oligodendrocytes and neurites as well as the spontaneously formed deposition of myelin segments in an aligned distribution.

One of the advantages in the microfluidics devices representing an open compartment design, like our design and the previously presented devices for myelination studies [13–16], include controlled cell seeding. In the enclosed compartment designs, cell seeding is commonly performed via inlet and outlet of the channel that easily leads to cell clogging in the channel or losing cells through outlet resulting in too low or high cell density [62]. As the open compartment design allows direct access to the compartments, it enables better control over the reproducibility of cell seeding in terms of cell number
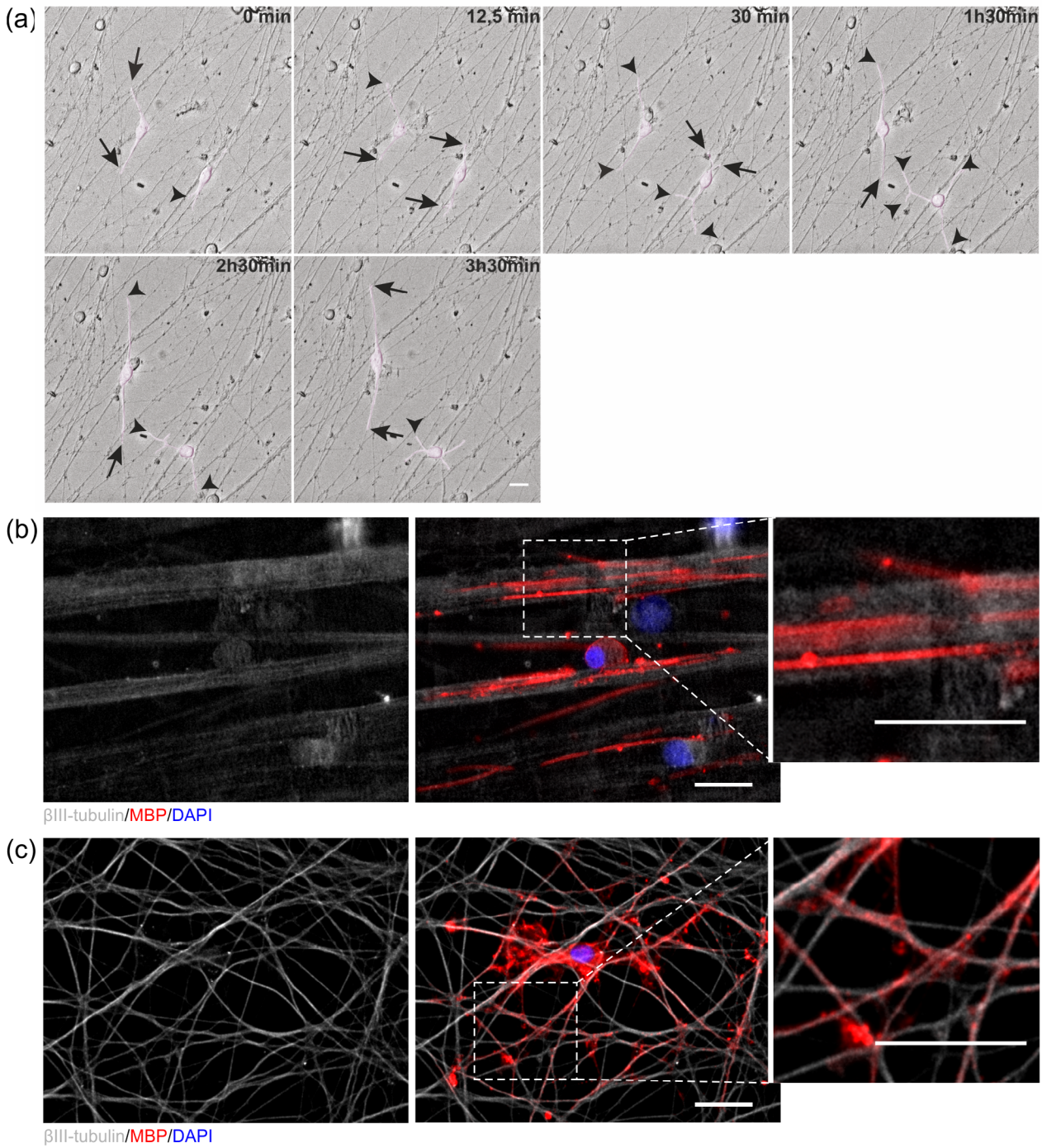
Figure 5. Myelination in the microfluidics device. (a) Selected still image frames from time-lapse imaging (see supplementary movie 1 from another position in the same device) of rat OPC processes contacting and surveying the neurites of rat DRG neurons (arrows). Arrowheads indicate the extension of OPC processes and OPCs are visualized using false colouring. (b) Oligodendrocytes formed MBP segments along the neurites with an oriented distribution in the microfluidics device as demonstrated by immunocytochemical labelling for βIII-tubulin and MBP. (c) The random MBP distribution along neurites in the control co-culture. Scale bars are 20 μm.

seeded in each compartment. The studies with enclosed compartment devices have also shown that the seeding and culture of e.g. embryonic bodies (EBs) of stem cells is impossible to the devices due to the shallow compartment height [20]. The open compartment devices bypass this problem and enable the possibility of culturing at least EBs, complete DRGs, DRG explants and 3D cell aggregates [20, 23, 63]. Replacement of enclosed compartments by open compartments has also led

to improved cell viability and neurite growth [4, 21, 22]. The problems in cell survival and axon extension in enclosed compartment devices employing inlet and outlet system [4, 21, 22] may arise from uncontrolled cell density or shear stress of cells during cell seeding and medium exchange even though careful techniques are used [8, 62]. Another possible cause may be inefficient or insufficient nutrient supply and waste removal that damage sensitive cells. If nutrient/waste exchange is

based on diffusion, it can take a long time in enclosed compartment devices. Furthermore, as culture area-to-volume ratio is much higher in enclosed compartments than in open compartments, the regular time interval between media changes may not be sufficient [8, 62]. Medium perfusion can be used in microfluidics devices to improve efficiency of nutrient/waste exchange [8, 62]. Controlled perfusion systems are almost always pump-driven because pumps give excellent flow control [64]. The major downside of the pump-driven flow is the need of additional equipment that complicates handling for end users and increases the change for problems, such as leakages at connection points [62]. The added value of our open compartment device is controlled cell seeding and efficient nutrient and waste product exchange without requirement of additional equipment. Thus, the device is easy to use and can be easily adopted to standard cell culture laboratories.

4. Conclusions

We created a compartmentalized microfluidics cell culture device targeted for the co-culturing of neurons and oligodendrocytes in myelin studies *in vitro*. The design of the device promoted the formation of aligned-oriented neurites in an isolated compartment. The device is advantageous over previously reported devices using rodent primary cells, as the spontaneous formation of MBP segments along neurites with an aligned distribution in a rat primary DRG neuron and oligodendrocyte co-culture was achieved.

To create a device with these benefits, we propose a novel fabrication method to produce PDMS-based microfluidics cell culture devices with open compartments. The method combines, for the first time, a photolithography process with 3D printing in the fabrication of a mould that replicates both the microscopic and macroscopic features for the PDMS device at the same time. The designed microscale features were replicated with high accuracy and devices were produced with good repeatability. Compared to existing methods reported for the fabrication of microfluidics devices with open compartments, our method provides a simple and effective way to produce complex moulds containing features in all sizes. We believe that the method can be widely used and adopted to easily fabricate a wide variety of PDMS devices for *in vitro* research purposes. Our fabrication method is unique and especially suitable for purposes where a large range of variation is needed in all three dimensions of the microfluidics device.

Among the advantages of the presented device is that it can be used for long-term live imaging with commercially available time-lapse imaging systems. Achieving a directional growth of neurites in the device gives benefits in the research questions where axonal biology is of interest. Aligned myelin distribution in a specific region of the device in the absence of neuronal cell somas facilitates the analysis of myelination. These features potentially allow for automated and quantitative analysis of myelination. Thus, the use of the proposed co-culture device may lead to a better understanding of myelination mechanisms both in health and disease and to the development of better treatments for diseases associated with myelin defects.

Supplementary data

Supplementary Movie 1. OPC processes contacting and surveying neurites in the rat DRG neuron and oligodendrocyte co-culture in the microfluidics device. Scale bar is 20 μm.

ORCID iDs

Mervi Ristola https://orcid.org/0000-0002-3748-3304
Lassi Sukki https://orcid.org/0000-0001-9181-7355
Maria Manuela Azevedo https://orcid.org/0000-0001-7316-8283
Ana Isabel Seixas https://orcid.org/0000-0003-3237-777X
João Bettencourt Relvas https://orcid.org/0000-0001-7636-0924
Susanna Narkilahti https://orcid.org/0000-0002-7602-4418
Pasi Kallio https://orcid.org/0000-0002-2890-6782

References

[1] Nave K and Werner H B 2014 *Annu. Rev. Cell Dev. Biol.* **30** 503–33
[2] Hosmane S, Yang I H, Ruffin A, Thakor N and Venkatesan A 2010 *Lab Chip* **10** 741–7
[3] Barbati A C, Fang C, Banker G A and Kirby B J 2013 *Biomed. Microdevices* **15** 97–108
[4] Kerman B E *et al* 2015 *Development* **142** 2213–25
[5] Osorio-Querejeta I, Sáenz-Cuesta M, Muñoz-Culla M and Otaegui D 2017 *Neuromolecular Med.* **19** 181–92
[6] Duncan I D and Radcliff A B 2016 *Exp. Neurol.* **283** 452–75

[7] Millet L J and Gillette M U 2012 *Yale J. Biol. Med.* **85** 501–21
[8] Halldorsson S, Lucumi E, Gómez-Sjöberg R and Fleming R M T 2015 *Biosens. Bioelectron.* **63** 218–31
[9] Siddique R and Thakor N 2014 *J. R. Soc. Interface* **11** 20130676
[10] Williamson J M and Lyons D A 2018 *Front. Cell. Neurosci.* **12** 424
[11] Campenot R B 1977 *Proc. Natl Acad. Sci. USA* **74** 4516–9
[12] Taylor A M, Blurton-Jones M, Rhee S W, Cribbs D H, Cotman C W and Jeon N L 2005 *Nat. Methods* **2** 599–605
[13] Park J, Koito H, Li J and Han A 2009 *Biomed. Microdevices* **11** 1145–53
[14] Park J, Koito H, Li J and Han A 2012 *Lab Chip* **12** 3296–304
[15] Yang I H, Gary D, Malone M, Dria S, Houdayer T, Belegu V, McDonald J W and Thakor N 2012 *Neuromolecular Med.* **14** 112–8
[16] Malone M, Gary D, Yang I H, Miglioretti A, Houdayer T, Thakor N and McDonald J 2013 *Glia* **61** 843–54
[17] Xie J, Willerth S M, Li X, Macewan M R, Rader A, Sakiyama-Elbert S E and Xia Y 2009 *Biomaterials* **30** 354–62
[18] Zhu Y, Wang A, Patel S, Kurpinski K, Diao E, Bao X, Kwong G, Young W L and Li S 2011 *Tissue Eng.* C **17** 705–15
[19] Walker G M, Zeringue H C and Beebe D J 2004 *Lab Chip* **4** 91–7
[20] Shin H S, Kim H J, Min S K, Kim S H, Lee B M and Jeon N L 2010 *Biotechnol. Lett.* **32** 1063–70
[21] Kim-Han J S, Antenor-Dorsey J A and O'Malley K L 2011 *J. Neurosci.* **31** 7212–21
[22] Lu X, Kim-Han J S, O'Malley K L and Sakiyama-Elbert S E 2012 *J. Neurosci. Methods* **209** 35–9
[23] van de Wijdeven R, Ramstad O H, Bauer U S, Halaas Ø, Sandvig A and Sandvig I 2018 *Biomed. Microdevices* **20** 9
[24] Park J, Li J and Han A 2010 *Biomed. Microdevices* **12** 345–51
[25] Yang I H, Siddique R, Hosmane S, Thakor N and Höke A 2009 *Exp. Neurol.* **218** 124–8
[26] Tsantoulas C, Farmer C, Machado P, Baba K, McMahon S B and Raouf R 2013 *PLoS One* **8** e80722
[27] Jia L, Wang L, Chopp M, Zhang Y, Szalad A and Zhang Z G 2016 *Neuroscience* **329** 43–53
[28] Pan L, Alagapan S, Franca E, Leondopulos S S, DeMarse T B, Brewer G J and Wheeler B C 2015 *Front. Neural. Circuits* **9** 32
[29] Xia Y and Whitesides G M 1998 *Angew. Chem., Int. Ed. Engl.* **37** 550–75
[30] Bremen S, Meiners W and Diatlov A 2012 *Laser Tech. J.* **9** 33–8
[31] Hemmilä S, Cauich-Rodríguez J V, Kreutzer J and Kallio P 2012 *Appl. Surf. Sci.* **258** 9864–75
[32] Azevedo M M, Domingues H S, Cordelières F P, Sampaio P, Seixas A I and Relvas J B 2018 *Glia* **66** 1826–44
[33] Laursen L S, Chan C W and Ffrench-Constant C 2011 *J. Cell Biol.* **192** 797–811
[34] McCarthy K D and de Vellis J 1980 *J. Cell Biol.* **85** 890–902
[35] Chen Y, Balasubramaniyan V, Peng J, Hurlock E C, Tallquist M, Li J and Lu Q R 2007 *Nat. Protocols* **2** 1044–51
[36] Wood P, Okada E and Bunge R 1980 *Brain Res.* **196** 247–52
[37] Wang Z, Colognato H and Ffrench-Constant C 2007 *Glia* **55** 537–45
[38] Schnädelbach O, Ozen I, Blaschuk O W, Meyer R L and Fawcett J W 2001 *Mol. Cell. Neurosci.* **17** 1084–93
[39] Johnson M I, Bunge R P and Wood P M 2001 Primary Cell Cultures for the Study of Myelination (New York, Humana Press) pp 95–115
[40] Edelstein A D, Tsuchida M A, Amodaj N, Pinkard H, Vale R D and Stuurman N 2014 *J. Biol. Methods* **1** e10
[41] Barateiro A, Miron V E, Santos S D, Relvas J B, Fernandes A, Ffrench-Constant C and Brites D 2013 *Mol. Neurobiol.* **47** 632–44
[42] Schindelin J *et al* 2012 *Nat. Methods* **9** 676–82
[43] Rezakhaniha R, Agianniotis A, Schrauwen J T C, Griffa A, Sage D, Bouten C V C, van de Vosse F N, Unser M and Stergiopulos N 2012 *Biomech. Model. Mechanobiol.* **11** 461–73
[44] Fonck E, Feigl G G, Fasel J, Sage D, Unser M, Rüfenacht D A and Stergiopulos N 2009 *Stroke* **40** 2552–6
[45] Kartasalo K, Pölönen R, Ojala M, Rasku J, Lekkala J, Aalto-Setälä K and Kallio P 2015 *BMC Bioinform.* **16** 344
[46] Toivanen M, Pelkonen A, Mäkinen M, Ylä-Outinen L, Sukki L, Kallio P, Ristola M and Narkilahti S 2017 *Front. Neurosci.* **11** 606
[47] Hyysalo A, Ristola M, Joki T, Honkanen M, Vippola M and Narkilahti S 2017 *Macromol. Biosci.* **17** 1600517
[48] Madsen M H, Feidenhans'l N A, Hansen P, Garnæs J and Dirscherl K 2014 *J. Micromech. Microeng.* **24** 127002
[49] Lake M, Narciso C, Cowdrick K, Storey T, Zhang S, Zartman J and Hoelzle D 2015 *Protocol Exch.* (https://doi.org/10.1038/protex.2015.069)
[50] Ruppen J, Wildhaber F D, Strub C, Hall S R R, Schmid R A, Geiser T and Guenat O T 2015 *Lab Chip* **15** 3076–85
[51] Sun M, Xie Y, Zhu J, Li J and Eijkel J C T 2017 *Anal. Chem.* **89** 2227–31
[52] Duffy D C, McDonald J C, Schueller O J and Whitesides G M 1998 *Anal. Chem.* **70** 4974–84
[53] Anderson J R, Chiu D T, Jackman R J, Cherniavskaya O, McDonald J C, Wu H, Whitesides S H and Whitesides G M 2000 *Anal. Chem.* **72** 3158–64
[54] Jarjour A A, Zhang H, Bauer N, Ffrench-Constant C and Williams A 2012 *Glia* **60** 1–12
[55] Liu R, Lin G and Xu H 2013 *PLoS One* **8** e60558
[56] Unsain N, Heard K N, Higgins J M and Barker P A 2014 *J. Vis. Exp.* e51795
[57] Peyrin J *et al* 2011 *Lab Chip* **11** 3663–73
[58] Dworak B J and Wheeler B C 2009 *Lab Chip* **9** 404–10
[59] Coquinco A, Kojic L, Wen W, Wang Y T, Jeon N L, Milnerwood A J and Cynader M 2014 *Mol. Cell. Neurosci.* **60** 43–52
[60] Taylor A M, Dieterich D C, Ito H T, Kim S A and Schuman E M 2010 *Neuron* **66** 57–68
[61] Gibson E M *et al* 2014 *Science* **344** 1252304
[62] Young E W K and Beebe D J 2010 *Chem. Soc. Rev.* **39** 1036–48
[63] Gluska S, Zahavi E E, Chein M, Gradus T, Bauer A, Finke S and Perlson E 2014 *PLoS Pathog.* **10** e1004348
[64] Byun C K, Abi-Samra K, Cho Y and Takayama S 2014 *Electrophoresis* **35** 245–57